

The role of angular momentum in general relativity: heuristic and covariant interpretations

Erick Pastén*

Departamento de Física, Universidad de Santiago de Chile,
Avenida Víctor Jara 3493, Estación Central, 9170124, Santiago, Chile

Claudia Álvarez Rojas†

Departamento de Física, Universidad Técnica Federico Santa María, Av. España 1680, Valparaíso, Chile

Norman Cruz‡

Departamento de Física, Universidad de Santiago de Chile,
Avenida Víctor Jara 3493, Estación Central, 9170124, Santiago, Chile

We examine the role of angular momentum in general relativity from both heuristic and fully covariant perspectives, with the aim of clarifying conceptual ambiguities that arise when Newtonian intuition is extrapolated into the relativistic regime. Focusing on free-fall dynamics in the Schwarzschild and Kerr spacetimes in the test-particle limit, we employ an effective-potential heuristic approach to isolate the roles of the specific energy E , specific angular momentum L , and black-hole spin a . Within this framework, we identify well-defined regions of parameter space in which the Kerr spacetime leads to stronger or weaker local radial infall than the Schwarzschild case at the same radius. By analysing the kinematics of infalling geodesic congruences, we show how these local regimes combine along complete trajectories to either enhance or reduce gravitational focusing. We then interpret these results within a covariant 1+3 description of general relativity, in terms of the expansion, shear and Raychaudhuri evolution of timelike congruences. We demonstrate that black-hole rotation systematically modifies the shear of infalling irrotational flows, even when the magnitude of the local expansion is reduced, and that this shear modulation governs the overall rate of focusing. Our work complements previous studies of relativistic infall by providing a unified energetic and geometric interpretation of how angular momentum and rotation can strengthen or weaken gravitational collapse relative to the non-rotating case.

I. INTRODUCTION

In Newtonian gravity, angular momentum plays a well-known role: it acts as a centrifugal barrier that opposes gravitational collapse and lengthens infall times. Much of our understanding of gravitationally bound systems, from stellar dynamics to large-scale structure formation [1], relies on this intuition. However, in General Relativity the situation is different. Energy, momentum, and motion itself gravitate, and their interplay can modify the effective forces experienced by test particles, particularly in regimes of strong curvature and relativistic kinematics [2–5]. From a broader perspective, a point that is rarely emphasized in standard treatments is the idea that motion can enhance gravity. This phenomenon is not unique to black-hole physics. In cosmology, [6] and [7] have shown that peculiar velocities and the associated energy fluxes can act as additional gravitational sources, strengthening the growth rate of inhomogeneities compared with Newtonian expectations. These results suggest that relativistic kinematics can influence characteristic growth rates and collapse times even when deviations from homogeneity are small.

Test particles in curved spacetimes provide a clean and controlled setting in which such effects can be isolated and studied in detail. In particular, the Schwarzschild and Kerr solutions offer ideal laboratories to investigate the role of angular momentum in relativistic dynamics, without the additional complications introduced by hydrodynamics, radiation, or feedback processes [8–12]. Previous studies have shown that rotation can significantly modify the local dynamics of infalling matter. For example, in the context of accretion flows onto rotating black holes, [13] demonstrated that the radial velocity of the flow can be enhanced for low specific angular momentum and high spin. These results already indicate that angular momentum in General Relativity does not always act as a purely

* erick.contreras@usm.cl

† claudia.alvarezr@usm.cl

‡ norman.cruz@usach.cl

repulsive agent, and that relativistic couplings between energy, angular momentum, and spacetime rotation can strengthen the effective gravitational pull under certain conditions.

In this work, we revisit this issue by studying the free fall of test particles in the Schwarzschild and Kerr spacetimes. Our goal is not to model realistic astrophysical systems, but rather to clarify, at a conceptual level, how relativistic angular-momentum couplings and frame dragging modify gravitational attraction relative to the Newtonian picture. Using an effective-potential approach, we identify well-defined regions of parameter space, spanned by $(r/M, a/L, E)$, in which the Kerr spacetime is locally more attractive or more repulsive, in an energetic sense, than Schwarzschild at the same radius. We then show how these local regimes combine along complete geodesic trajectories to either shorten or lengthen the total proper infall time toward selected representative radii.

To place these results on a firm relativistic footing, we complement the heuristic effective-potential analysis with a fully covariant 1+3 description of the dynamics. In particular, we interpret the differences in infall times in terms of the expansion and focusing properties of timelike geodesic congruences, as governed by the Raychaudhuri equation. This covariant viewpoint clarifies how black-hole rotation modifies the balance between kinematic focusing and tidal distortion, and provides a direct link between angular momentum, spacetime geometry, and characteristic collapse times.

Although idealized, this analysis provides a transparent relativistic classification of when angular momentum strengthens or weakens gravitational attraction in Kerr spacetimes. As motivation, we note that recent discussions of unexpectedly short assembly times for massive structures have renewed interest in mechanisms capable of modifying effective growth timescales [14, 15]. In this context, our results offer a controlled General Relativistic benchmark for assessing how purely kinematic and geometric effects may contribute, alongside more complex astrophysical processes, to the timing of gravitational collapse.

II. FREE-FALL IN SCHWARZSCHILD AND KERR BLACK HOLES

We work in geometric units $G = c = 1$ and signature $(-, +, +, +)$. Timelike geodesics follow from the Lagrangian $\mathcal{L} = \frac{1}{2}g_{\mu\nu}\dot{x}^\mu\dot{x}^\nu$ with normalization $g_{\mu\nu}\dot{x}^\mu\dot{x}^\nu = -1$ (see e.g. [2–4]). Stationarity and axial symmetry imply two conserved quantities along the motion, the specific energy $E \equiv -p_t$ and azimuthal specific angular momentum $L \equiv p_\phi$, associated with the Killing vectors ∂_t and ∂_ϕ .

A. Schwarzschild: effective potential and benchmark times

The Schwarzschild line element is [8]

$$ds^2 = -\left(1 - \frac{2M}{r}\right)dt^2 + \left(1 - \frac{2M}{r}\right)^{-1}dr^2 + r^2(d\theta^2 + \sin^2\theta d\phi^2). \quad (1)$$

Without loss of generality we restrict to equatorial motion $\theta = \pi/2$. The conserved quantities can be written as

$$E = \left(1 - \frac{2M}{r}\right)\dot{t}, \quad L = r^2\dot{\phi}, \quad (2)$$

and the radial equation takes the effective-potential form

$$\dot{r}^2 = E^2 - V_{\text{eff}}^{\text{Schw}}(r; L), \quad V_{\text{eff}}^{\text{Schw}}(r; L) = \left(1 - \frac{2M}{r}\right)\left(1 + \frac{L^2}{r^2}\right). \quad (3)$$

Expanding the potential makes explicit the Newtonian limit and the leading relativistic correction,

$$V_{\text{eff}}^{\text{Schw}}(r; L) = 1 - \frac{2M}{r} + \frac{L^2}{r^2} - \frac{2ML^2}{r^3}, \quad (4)$$

where the last term is purely relativistic and enhances the effective attraction at small radii. Circular equatorial orbits which have zero radial velocity, satisfy $E^2 = V_{\text{eff}}$ and $dV_{\text{eff}}/dr = 0$, while stability is determined by d^2V_{eff}/dr^2 (see e.g. [3, 12]).

For an ingoing trajectory ($\dot{r} < 0$), the proper infall time from r_0 to r_f is

$$\Delta\tau(r_0 \rightarrow r_f) = \int_{r_f}^{r_0} \frac{dr}{\sqrt{E^2 - V_{\text{eff}}(r)}}. \quad (5)$$

The corresponding coordinate time follows from $dt/d\tau = E/(1 - 2M/r)$, giving

$$\Delta t(r_0 \rightarrow r_f) = \int_{r_f}^{r_0} \frac{E dr}{(1 - \frac{2M}{r}) \sqrt{E^2 - V_{\text{eff}}(r)}}. \quad (6)$$

In Schwarzschild coordinates Δt diverges as $r_f \rightarrow 2M$, while $\Delta\tau$ remains finite, as is well known.

Before turning to Kerr, it is useful to establish a Schwarzschild baseline by comparing relativistic and Newtonian infall times for the same initial conditions. Figure 1 shows the ratio $\Delta t_{\text{Newt}}/\Delta\tau_{\text{GR}}$ as a function of L for infall from r_0 to $6M$ (which corresponds to the innermost stable circular orbit (ISCO) in Schwarzschild spacetime) for a particle starting with zero radial velocity. As the particle angular momentum increases, the Newtonian infall time grows faster than the relativistic proper time. In other words, for fixed (r_0, r_f) and comparable angular-momentum values, General Relativity predicts a shorter proper collapse time than Newtonian intuition would suggest.

This trend is made explicit in Fig. 1. The systematic departure from unity at larger L is consistent with the structure of Eq. (3): while the term L^2/r^2 acts as a centrifugal barrier, the relativistic correction $-2ML^2/r^3$ partially counteracts it at smaller radii, reducing the proper infall time relative to the Newtonian prediction. This Schwarzschild result motivates our main Kerr question: once spacetime rotation is included, can the additional a -dependent couplings further strengthen (or weaken) the effective attraction and thereby shorten (or lengthen) the integrated infall time?

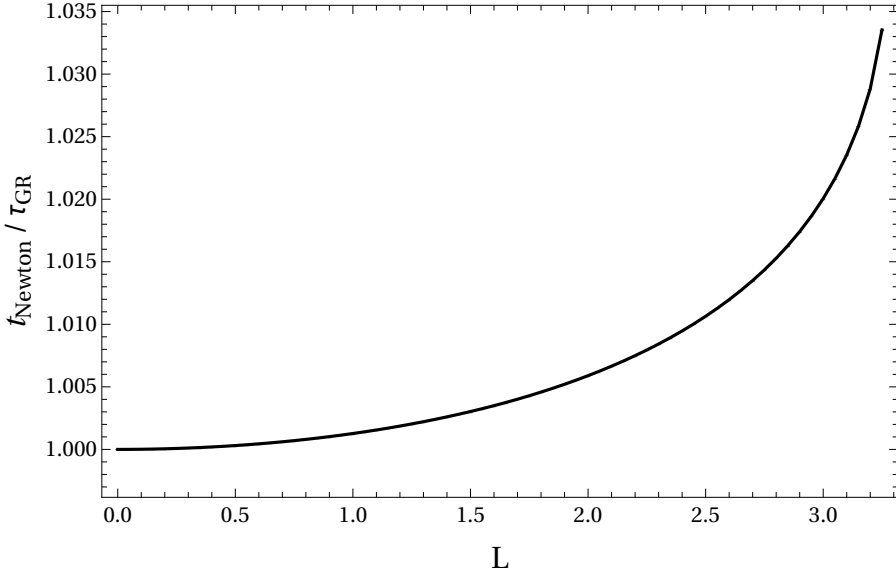


Figure 1: Ratio between the Newtonian infall time and the Schwarzschild proper infall time for trajectories from r_0 to $r_f = 6M$, as a function of angular momentum L . The increasing deviation from unity quantifies the relativistic reduction of the integrated proper fall time relative to Newtonian expectations.

B. Kerr: equatorial geodesics and spin-dependent couplings

The Kerr metric in Boyer–Lindquist coordinates is [9, 10]

$$\begin{aligned} ds^2 = & - \left(1 - \frac{2Mr}{\Sigma} \right) dt^2 - \frac{4Mar \sin^2 \theta}{\Sigma} dt d\phi + \frac{\Sigma}{\Delta} dr^2 + \Sigma d\theta^2 \\ & + \left(r^2 + a^2 + \frac{2Ma^2r \sin^2 \theta}{\Sigma} \right) \sin^2 \theta d\phi^2, \end{aligned} \quad (7)$$

with $\Sigma = r^2 + a^2 \cos^2 \theta$ and $\Delta = r^2 - 2Mr + a^2$. We focus on equatorial motion $\theta = \pi/2$, for which $\Sigma = r^2$ and the Carter constant vanishes ($Q = 0$; [11]). Conserved quantities are defined by

$$E = -p_t, \quad L = p_\phi, \quad p_\mu = g_{\mu\nu} \dot{x}^\nu. \quad (8)$$

Solving the (t, ϕ) system yields $\dot{t}(E, L)$ and $\dot{\phi}(E, L)$ (e.g. [12, 16]), and the radial equation can be written in a compact form as

$$\dot{r}^2 = (E^2 - 1) + \frac{2M}{r} + \frac{a^2(E^2 - 1) - L^2}{r^2} + \frac{2M(aE - L)^2}{r^3}, \quad (9)$$

which reduces to the Schwarzschild expression when $a \rightarrow 0$. Equation (9) highlights two distinct ways in which rotation modifies the dynamics relative to Schwarzschild. First, it introduces an explicit $a^2(E^2 - 1)/r^2$ contribution that reshapes the effective barrier. Second, the frame-dragging coupling appears through $(aE - L)^2$ in the $1/r^3$ term, breaking the symmetry under $L \rightarrow -L$ and implying different behaviour for co-rotating ($L > 0$) and counter-rotating ($L < 0$) trajectories.

The proper infall time in Kerr follows directly from the equatorial radial equation, Eq. (9). For an ingoing trajectory ($\dot{r} < 0$) we write

$$\frac{dr}{d\tau} = -\sqrt{\mathcal{R}(r; E, L, a)}, \quad \mathcal{R}(r; E, L, a) \equiv (E^2 - 1) + \frac{2M}{r} + \frac{a^2(E^2 - 1) - L^2}{r^2} + \frac{2M(aE - L)^2}{r^3}, \quad (10)$$

which can be equivalently cast in an effective-potential form $\dot{r}^2 = E^2 - V^{\text{Kerr}}$, with $V^{\text{Kerr}}(r; E, L, a) \equiv E^2 - \mathcal{R}(r; E, L, a)$. Inverting Eq. (10) gives an expression for the accumulated proper time between an initial radius r_0 and a final radius $r_f < r_0$,

$$\Delta\tau(r_0 \rightarrow r_f; E, L, a) = \int_{r_f}^{r_0} \frac{dr}{\sqrt{\mathcal{R}(r; E, L, a)}}, \quad (11)$$

which is finite for any r_f outside the event-horizon and is evaluated numerically throughout this work. When $a \rightarrow 0$, \mathcal{R} reduces to the Schwarzschild expression and Eq. (11), reproducing the curve shown in Fig 1.

III. HEURISTIC ANALYSIS

Before presenting infall times, it is useful to build intuition for how Kerr can behave as effectively more attractive or more repulsive than Schwarzschild for the same orbital parameters. Our strategy is to work directly at the level of the equatorial radial dynamics, rewrite it in a mechanical form, and then diagnose the sign and relative strength of the spin-dependent contributions.

The radial equation governing the motion of a particle in the equatorial plane of Kerr is

$$\dot{r}^2 = \frac{R(r)}{r^4}, \quad (12)$$

where

$$R(r) = \left[E(r^2 + a^2) - aL \right]^2 - \Delta \left[r^2 + (L - aE)^2 \right]. \quad (13)$$

We will cast this equation into a “Newtonian mechanical” form as

$$\frac{1}{2} \dot{r}^2 + V_{\text{eff}}(r; M, L, a, E) = \frac{E^2 - 1}{2}, \quad (14)$$

where the effective potential reads

$$V_{\text{eff}}(r; M, L, a, E) = -\frac{M}{r} + \frac{L^2}{2r^2} + \frac{a^2(1 - E^2)}{2r^2} - \frac{M(L - aE)^2}{r^3}. \quad (15)$$

Equation (14) admits an interpretation closely analogous to Newtonian mechanics: the first term on the left-hand side plays the role of radial *kinetic energy*, while V_{eff} acts as an effective gravitational potential that encapsulates

the geometric effects of the spacetime in the radial sector. The right-hand side, $(E^2 - 1)/2$, controls whether the motion is bound or unbound. For a unit-mass particle ($m = 1$), it measures the deviation between the total specific energy and the rest-mass energy; orbits with $E < 1$ are bound, while $E > 1$ corresponds to unbound trajectories or scattering motion. This reading is particularly useful for our purposes: at fixed radius, an *increase* in V_{eff} tends to *reduce* the radial speed \dot{r} , and therefore suggests longer infall times once the dynamics is integrated along complete trajectories. Conversely, regions of parameter space in which V_{eff} becomes more negative correspond to a more “attractive” radial dynamics (in the sense of a larger radial acceleration / larger \dot{r}), foreshadowing systematically shorter integrated proper times. This mechanism has been explored previously in [13], where it is shown that black-hole rotation can increase the radial velocity of the flow, particularly for low-angular-momentum configurations and high spin.

The form (15) is especially convenient because it separates the net Kerr contribution into four terms with clear physical meaning:

1. **Classical gravity:** the term $-M/r$ reproduces the Newtonian gravitational attraction associated with the black-hole mass.
2. **Centrifugal barrier:** the term $L^2/(2r^2)$ is the classical centrifugal barrier associated with the particle’s orbital angular momentum. It is repulsive and inhibits radial infall.
3. **Spin–energy coupling:** the term $a^2(1-E^2)/(2r^2)$ is purely relativistic and has no analogue in Schwarzschild. Its sign depends on whether the orbit is bound ($E < 1$) or unbound ($E > 1$), modifying the intermediate-radius structure of the potential. Its magnitude increases with larger a .
4. **Spin–orbit–energy coupling:** the term $-M(L-aE)^2/r^3$ encodes an attractive contribution produced by the particle’s angular momentum, but corrected by a factor aE . This term can be understood by introducing the *effective angular momentum*

$$L_{\text{eff}} = L - aE,$$

which measures the mismatch between the particle’s own angular momentum and the angular-momentum “drag” induced by the black hole rotation.

This decomposition makes it transparent why Kerr can display qualitatively different behavior from Schwarzschild even at fixed L : the appearance of $L - aE$ means that frame dragging can compete directly with the classical centrifugal barrier, and that competition is amplified or suppressed depending on the energy and on the relative sign between a and L (co-rotation versus counter-rotation).

A. Analysis of particular cases

To gain deeper insight into the terms appearing in the effective potential, it is useful to consider a few limiting cases. These limits are of course not exhaustive, but they are sufficient to isolate the mechanisms that matter for the discussion below. The principal mechanisms are: how L enters in a non-rotating space-time, how spin affects the dynamics even when the particle carries no intrinsic angular momentum and how the balance behaves at the critically bound trajectory. Together, these cases serve as anchors for interpreting the general Kerr behavior.

1. Schwarzschild black hole ($a = 0$)

In the absence of rotation, the effective potential reduces to

$$V_{\text{eff}}(r; M, L, a = 0, E) = -\frac{M}{r} + \frac{L^2}{2r^2} - \frac{ML^2}{r^3}. \quad (16)$$

In this case, the particle’s angular momentum does not only act as a centrifugal barrier (the term $L^2/(2r^2)$), but also contributes to gravitational attraction through the term $-ML^2/r^3$, which is reflected in the figure 1 presented in the previous section. This latter term originates from the curvature of Schwarzschild spacetime: in General Relativity, the energy associated with orbital motion contributes effectively to gravitation, modifying the radial dynamics even for a test particle. The net contribution of L to the relativistic radial dynamics can be described by

$$V_L(r) = \frac{L^2}{2r^2} \left(1 - \frac{2M}{r}\right). \quad (17)$$

For $r > 2M$, the factor in parentheses is strictly positive, hence $V_L(r) > 0$ throughout the entire region exterior to the event horizon. Therefore, the net effect of angular momentum remains a centrifugal barrier in General Relativity, albeit attenuated by the attractive relativistic correction proportional to $-ML^2/r^3$. This correction does not flip the sign of V_L outside the horizon, but it does reduce its magnitude compared to the purely Newtonian barrier. In Schwarzschild, unlike Kerr, there is no possibility for the L -associated effective contribution to become attractive outside the horizon. This already suggests that any effective “inversion” of the classical centrifugal barrier (in the sense of net attractive angular-momentum contributions) must arise from the a -dependent Kerr terms.

2. Particle with no intrinsic angular momentum ($L = 0$)

A particle with vanishing intrinsic angular momentum moves under the effective potential

$$V_{\text{eff}}(r; M, L = 0, a, E) = -\frac{M}{r} + \frac{a^2(1 - E^2)}{2r^2} - \frac{Ma^2E^2}{r^3}. \quad (18)$$

In addition to the Newtonian term $-M/r$, two purely relativistic contributions appear. The term proportional to Ma^2E^2/r^3 is negative and therefore always increases the net attraction. Thus, we again encounter the notion that motion “gravitates,” now mediated by the black-hole spin parameter a and the particle energy E . This is important because it shows that rotation can modify the radial dynamics even in the absence of a classical centrifugal barrier ($L = 0$).

On the other hand, the term $a^2(1 - E^2)/(2r^2)$ changes sign depending on the energy: for bound motion ($E < 1$) it is positive and repulsive, while for unbound motion ($E > 1$) it becomes negative and thus attractive. The global effect of the relativistic spin corrections can be assessed by grouping both terms into

$$V_a(r; E) = a^2 \left(\frac{1 - E^2}{2r^2} - \frac{ME^2}{r^3} \right), \quad (19)$$

which represents the part of the effective potential that vanishes when the rotation is switched off ($a = 0$). The sign of V_a determines whether the total spin-induced relativistic correction is net repulsive ($V_a > 0$) or net attractive ($V_a < 0$). (Note that this is a local diagnostic at a given radius.)

Defining the critical energy

$$E_a(r) \equiv \sqrt{\frac{r}{r + 2M}}, \quad (20)$$

we can summarize the behavior as

$$E < E_a(r) \implies V_a(r; E) > 0 \quad (\text{net repulsive relativistic correction}), \quad (21)$$

$$E > E_a(r) \implies V_a(r; E) < 0 \quad (\text{net attractive relativistic correction}). \quad (22)$$

From these equations we see that $E_a(r) < 1$ for all $r > 0$, and that $E_a(r) \rightarrow 1$ as $r \rightarrow \infty$. In particular, for particles with $E > 1$ (unbound motion) one always has $E^2 > r/(r + 2M)$, so $V_a(r; E)$ is strictly negative and the spin-induced relativistic contribution is net attractive at any radius. On the other hand, since $E_a(r)$ decreases toward smaller radii, sufficiently close to the event horizon it becomes possible for black-hole rotation to yield a net attractive effect even for bound motion (see Table 1). This point is conceptually important: even when $E < 1$, spin can tip the balance toward attraction at small radii, underscoring that the impact of a must always be assessed in conjunction with the radial domain effectively sampled by the trajectory.

3. Critically bound motion ($E = 1$)

For a particle with critically bound energy ($E = 1$), the effective potential reduces to

$$V_{\text{eff}}(r; M, L, a, E = 1) = -\frac{M}{r} + \frac{L^2}{2r^2} - \frac{M(L - a)^2}{r^3}. \quad (23)$$

Table I: Values of the critical energy $E_a(r) = \sqrt{r/(r+2M)}$ for different radii (with $M = 1$). For $E > E_a(r)$ the spin-induced relativistic contribution (V_a) is net attractive.

r/M	$E_a(r)$
100	0.9950
20	0.9535
10	0.9129
6	0.8452
5	0.8165
4	0.7746
3	0.7071

Here we again find the Newtonian term $-M/r$ together with a classical centrifugal barrier, $L^2/(2r^2)$, now corrected by a purely relativistic attractive term proportional to $-(L-a)^2/r^3$. This term can be interpreted as a *spin-orbit coupling*, where the combination $L_{\text{eff}} = L - a$ plays the role of an effective angular momentum in the presence of frame dragging.

The net contribution of angular momentum to the radial dynamics for $E = 1$ is then contained in

$$V_{L,a}(r) = \frac{L^2}{2r^2} - \frac{M(L-a)^2}{r^3}. \quad (24)$$

Its sign determines whether the overall effect of angular momentum is predominantly repulsive ($V_{L,a} > 0$) or attractive ($V_{L,a} < 0$). Writing

$$V_{L,a}(r) = \frac{1}{2r^3} \left[rL^2 - 2M(L-a)^2 \right], \quad (25)$$

the condition $V_{L,a} = 0$ becomes

$$r - 2M \left(1 - \frac{a}{L} \right)^2 = 0. \quad (26)$$

It is useful to define the angular-momentum ratio $\lambda = \frac{a}{L}$, where $\lambda > 0$ corresponds to co-rotating motion while $\lambda < 0$ corresponds to counter-rotating motion. Likewise, $|\lambda| \ll 1$ indicates a slowly rotating black hole compared to the particle's angular momentum, while $|\lambda| \gg 1$ indicates the opposite. Moreover, since $a < M$ by cosmic censorship, one has $\lambda < M/L$ in all cases. For $r > 2M$ the above equation admits two real solutions for the critical value:

$$\lambda_c^\pm(r) = 1 \pm \sqrt{\frac{r}{2M}}. \quad (27)$$

Values of λ in the interval $[\lambda_c^-(r), \lambda_c^+(r)]$ yield a net repulsive contribution, while values outside that interval increase the net attraction. From Table II one can infer that at large radii one would need $|a|$ to dominate strongly over $|L|$ to produce a net attractive effect, while this requirement weakens at smaller radii. Counter-rotating orbits have a broader parameter domain where the contribution can become attractive, because the repulsive interval is slightly shifted toward positive λ . Frame dragging therefore shifts the balance between angular-momentum terms and breaks the co-rotating/counter-rotating symmetry present in Schwarzschild. Note in particular that near the event horizon attraction dominates for all counter-rotating orbits.

From these three limiting cases we see that General Relativity introduces a substantially richer dynamics than the Newtonian one: the interplay between the classical centrifugal barrier and the a -dependent relativistic terms produces attractive and repulsive regimes that depend sensitively on how the particle parameters compete with the black-hole spin and on which radial region the orbit actually samples. This motivates the analysis of the fully general case.

B. Analysis of the general case

The effective potential in the fully general case is

$$V_{\text{eff}}(r; M, L, a, E) = -\frac{M}{r} + \frac{L^2}{2r^2} + \frac{a^2(1-E^2)}{2r^2} - \frac{M(L-aE)^2}{r^3}. \quad (28)$$

Table II: Values of $\lambda_c^\pm(r)$ for $M = 1$. For $\lambda_- < \lambda < \lambda_+$ the combined angular-momentum contribution to the effective potential ($V_{L,a}$) is net repulsive, whereas for $\lambda < \lambda_-$ or $\lambda > \lambda_+$ it is net attractive.

r/M	λ_-	λ_+
2	0	2
3	-0.2247	2.2247
4	-0.4142	2.4142
5	-0.5811	2.5811
6	-0.7321	2.7321
10	-1.2361	3.2361
20	-2.1623	4.1623
100	-6.0711	8.0711

From the effective-potential viewpoint, the specific energy E plays a dual role in Kerr. First, it controls the sign of the purely spin-associated term

$$\frac{a^2(1-E^2)}{2r^2}, \quad (29)$$

which is repulsive for bound motion ($E < 1$), vanishes at the critical case ($E = 1$), and becomes attractive for unbound motion ($E > 1$). Second, E enters the spin-orbit combination $L - aE$ appearing in

$$-\frac{M(L-aE)^2}{r^3}, \quad (30)$$

so that the dimensionless ratio

$$\mu \equiv \frac{aE}{L} \quad (31)$$

controls how effectively the black-hole rotation can compete with the classical centrifugal barrier. For $|\mu| \ll 1$ one recovers a Schwarzschild-like regime dominated by $L^2/(2r^2)$, whereas $|\mu| \gg 1$ corresponds to a relativistic regime in which the $(L - aE)^2$ term can render the dynamics more attractive than in the non-rotating case, especially at small radii. In this sense, increasing energies amplify the impact of spin on orbital dynamics and broaden the parameter domain in which relativistic corrections manifest as a net enhancement of gravitational attraction. At the same time, the same mechanism naturally introduces a strong asymmetry between co-rotating and counter-rotating motion, because the relative sign between a and L determines whether $L_{\text{eff}} = L - aE$ is reduced or increased.

To isolate exclusively the spin-induced contribution of Kerr, it is convenient to consider the difference between the Kerr and Schwarzschild effective potentials:

$$V_\Delta(r) \equiv V_{\text{eff}}^{\text{Kerr}} - V_{\text{eff}}^{\text{Schw}}. \quad (32)$$

Using the general expression, this difference can be written as

$$V_\Delta(r) = \frac{a^2(1-E^2)}{2r^2} - \frac{M[(L-aE)^2 - L^2]}{r^3}. \quad (33)$$

Expressing it in terms of the dimensionless ratio $\lambda = a/L$ and normalizing by L^2 yields

$$\frac{V_\Delta(r; \lambda, E)}{L^2} = \frac{\lambda^2(1-E^2)}{2r^2} + \frac{2M\lambda E - M\lambda^2 E^2}{r^3}. \quad (34)$$

The quantity V_Δ provides a direct diagnostic of whether, at a given radius, black-hole rotation makes the dynamics more attractive or more repulsive than in Schwarzschild. Since this criterion is local, it should be read as a tendency indicator which, once integrated along the full trajectory, will translate into systematically shorter or longer infall times depending on which radial region is effectively sampled.

We can then define a critical energy $E_{\text{crit}}^\Delta(r, \lambda)$ by imposing

$$V_\Delta(r; \lambda, E) = 0, \quad (35)$$

which leads to a quadratic equation in E whose solution is

$$E_{\text{crit},\Delta}(r, \lambda) = \frac{2Mr \pm \sqrt{r(4M^2r + \lambda^2r(r + 2M))}}{\lambda(r + 2M)}. \quad (36)$$

we choose the physically relevant root ensuring $E_{\text{crit},\Delta} > 0$. For $E > E_{\text{crit},\Delta}$ the Kerr potential is more attractive than the Schwarzschild one at that radius, while for $E < E_{\text{crit},\Delta}$ the net spin effect is repulsive.

Representative values of $E_{\text{crit},\Delta}$ are shown in Table III. For small $|\lambda|$ ($L \gg a$) in co-rotating motion, the critical energy lies in the unbound regime, indicating that rotation cannot compensate the centrifugal barrier. For large $|\lambda|$ ($a \gtrsim L$), $E_{\text{crit},\Delta}$ decreases, widening the energy domain for which Kerr is more attractive than Schwarzschild. Moreover, for counter-rotating motion ($\lambda < 0$) one obtains systematically smaller values of $E_{\text{crit},\Delta}$, implying a broader parameter domain in which black-hole rotation enhances the net attraction.

Table III: Representative values of the critical energy $E_{\text{crit},\Delta}(r, \lambda)$ for $M = 1$, different radii r/M and dimensionless ratios $\lambda = a/L$. For $E > E_{\text{crit},\Delta}$ the Kerr potential is more attractive than the Schwarzschild one at that radius.

r/M	$\lambda = -2$	$\lambda = -1$	$\lambda = 1$	$\lambda = 2$
3	0.53	0.20	1.18	0.97
4	0.62	0.33	1.16	0.99
5	0.67	0.43	1.15	1.01
6	0.71	0.50	1.14	1.02
10	0.81	0.67	1.11	1.05
20	0.90	0.82	1.08	1.07

For a fixed energy one can also define a critical radius r_{crit} separating attractive and repulsive regimes. Imposing again $V_{\Delta}(r_{\text{crit}}) = 0$ and solving for r yields

$$\frac{r_{\text{crit}}}{M} = \frac{2(E\lambda - 2)}{\lambda(1 - E^2)}. \quad (37)$$

This expression defines the radial boundary between regions where Kerr rotation makes the effective potential more attractive or more repulsive than in Schwarzschild, a boundary that appears explicitly in the diagrams shown in Fig. 2.

IV. INTEGRATED TIMES

The heuristic analysis presented in the previous section provides a local characterization of the attractive or repulsive nature of the effective potential in Kerr spacetime as a function of radius and dynamical parameters. A freely infalling particle, however, does not remain confined to a single local regime, but instead traverses a sequence of regions with different effective behavior, whose cumulative contribution determines the global dynamics of the motion. Consequently, in order to assess the net impact of these local regimes, it is necessary to consider infall times integrated along complete trajectories.

To this end, we use Eq. (11) to compute the proper time required for a test particle to fall from a fixed initial radius $r_0 = 10M$ down to a final radii $r_f = 3M$, exploring how the physical parameters of the system affect the integrated dynamics. The corresponding infall times are shown in Fig. 3. In this case, the infall time decreases systematically with increasing spin a for counter-rotating orbits, while it increases with a for corotating orbits, independently of whether the time is normalized or not. This behavior is fully consistent with the attractive and repulsive regimes identified in the heuristic analysis of the effective potential, confirming that the integrated dynamics faithfully reflects the local structure of the potential.

We have also computed infall times for a fixed final radius $r_f = 6M$ and verified that the qualitative trends are identical to those found for $r_f = 3M$. Since the $6M$ case does not introduce additional physical insight, we omit those curves for conciseness.

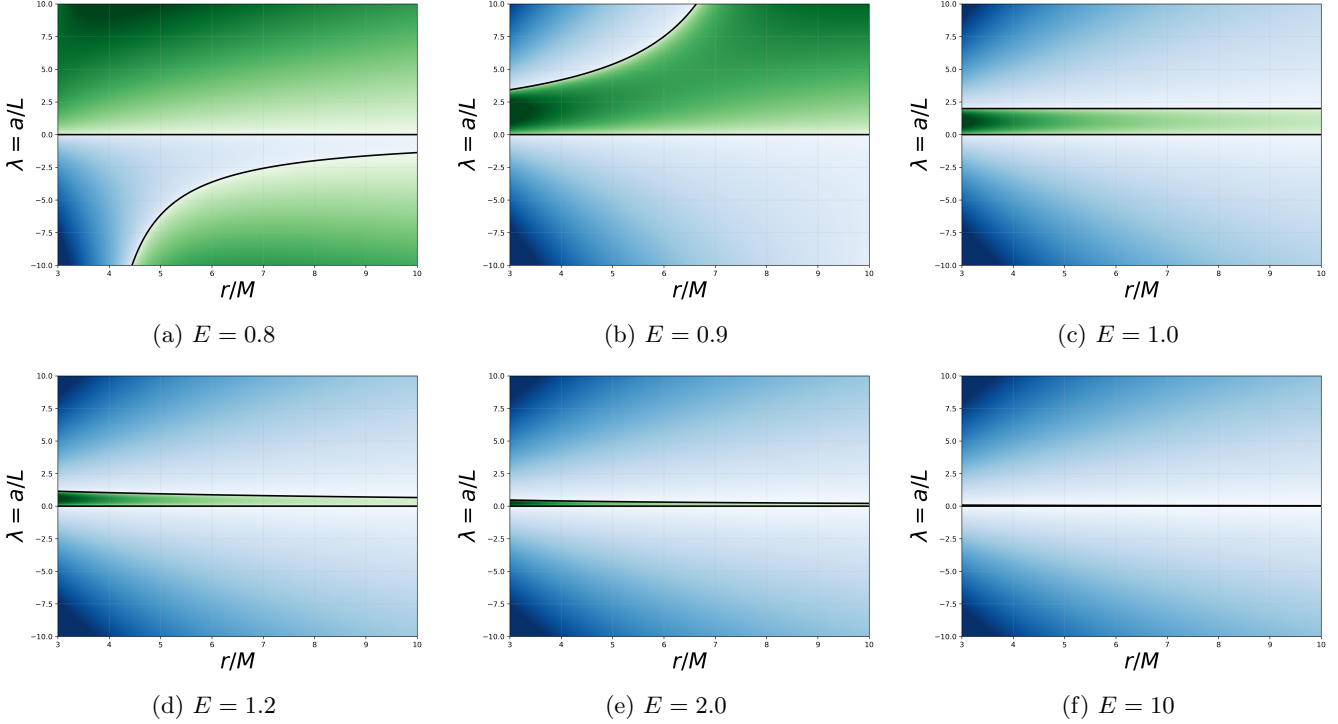


Figure 2: Maps of the Kerr spin-induced deviation of the effective potential from Schwarzschild, $V_\Delta(r; \lambda)/L^2$, shown as a function of the dimensionless radius r/M (horizontal axis) and the parameter $\lambda = a/L$ (vertical axis), for different values of the energy E . Blue regions correspond to a regime that is more attractive than Schwarzschild, while green regions correspond to a more repulsive regime. Note the sharp transition between co-rotating and counter-rotating motion in the limiting case $\lambda = 0$, where the regime switches from repulsive to attractive. At high energies, Kerr rotation yields a more attractive regime than Schwarzschild over essentially the entire parameter space.

A. Energetic versus rotational origin of the reduction in τ

The numerical results above show that the proper infall time decreases substantially as the particle specific energy E increases. This trend is already present in Schwarzschild (and has a direct Newtonian analogue) and follows from the radial equation of motion: increasing E raises the dominant contribution to \dot{r}^2 , thereby reducing the integrand $1/\sqrt{\dot{r}^2}$ in the proper-time integral. A significant fraction of the reduction in τ is therefore of purely energetic origin. This raises a key question for Kerr: to what extent is the shorter infall time a genuinely rotational effect, rather than a trivial consequence of injecting more energy into the trajectory?

To isolate the rotational contribution, we compare Kerr and Schwarzschild directly for fixed endpoints ($r_0 = 10M$ and $r_f = 3M$), keeping the angular momentum L fixed and varying only the energy E (Fig. 4). We consider the ratio $\tau_{\text{Kerr}}/\tau_{\text{Schw}}$, which factor out the dominant energetic dependence and highlight the net correction due to spin. For sufficiently large E , the ratio $\tau_{\text{Kerr}}/\tau_{\text{Schw}}$ does not approach unity; instead, it saturates at a constant value below one, set by the rotation parameter a . This demonstrates that Kerr rotation introduces a systematic correction—subdominant compared to the energetic effect, but physically robust—that further shortens the proper infall time relative to the non-rotating case. The same qualitative behavior appears for both corotating and counter-rotating families, and it persists even when the explicit dependence on the sign of L becomes secondary at high energies.

B. From local regimes to integrated infall times

The numerical trends discussed above can be interpreted coherently in light of the heuristic analysis of the effective potential. It is important to stress, however, that the heuristic classification is *local*: for each point in parameter

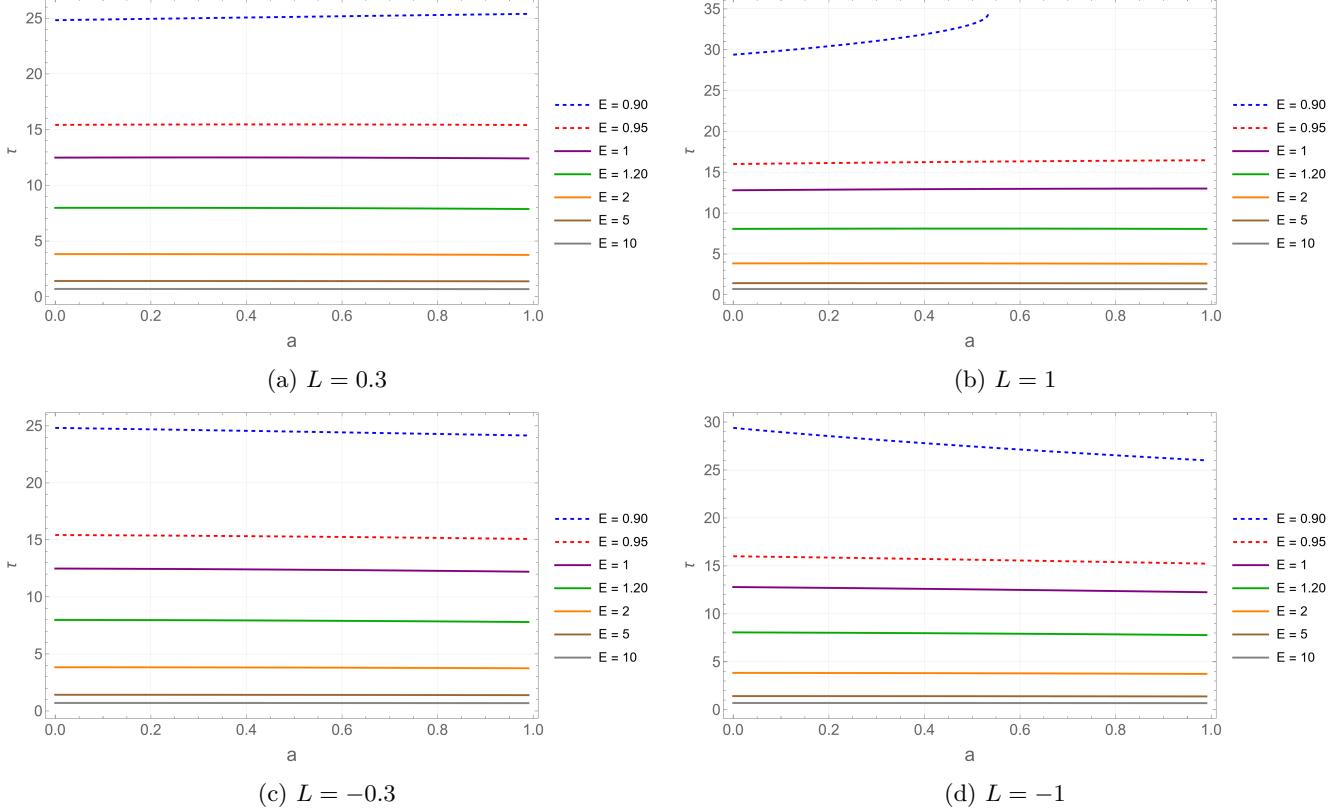


Figure 3: Profiles of τ as a function of the spin parameter a for prograde (UP) and retrograde (DOWN) infall down to a fixed radius $r_f = 3M$. Curves are shown for several values of the specific energy E and for two representative angular momenta, $L = 0.3$ and $L = 1$. For low and moderate energies, τ increase markedly with a for prograde orbits, while the trend is the opposite for retrograde trajectories. At higher energies, the overall infall time is shorter and becomes nearly independent of the black-hole spin.

space and each radius, it identifies whether the angular-momentum sector of the potential contributes effectively as an attractive or repulsive term in the radial dynamics. By contrast, the infall times are *integrated* quantities computed along complete trajectories, which necessarily sweep across multiple local regimes.

This is illustrated explicitly in Fig. 5, which shows parametric maps of the sign and magnitude of the normalized Kerr-minus-Schwarzschild potential variation in the $(r/M, \lambda = a/L)$ plane, together with representative infall tracks (dotted black curves) starting at $r_0 = 10M$ and moving inward. Each panel also displays the event horizon (solid red curve), the corotating or counter-rotating ISCO (dashed red curves), and reference fixed radii (vertical dashed white lines).

A first key point is that increasing a does not keep a given trajectory within a single dynamical regime. Instead, as $\lambda = a/L$ varies, the same family can cross locally more or less attractive and more or less repulsive regions before reaching the final radius. The global trend of the integrated infall time is therefore not dictated solely by the presence of an attractive or repulsive domain, but by *how much of the radial interval* is spent in each regime, *where* those regimes are located along the trajectory and *how* strong the regime is.

This is particularly clear at low energies and moderate-to-large angular momenta. For instance, for $E = 0.9$ and $L = 0.3$, corotating families ($\lambda > 0$) traverse an increasing fraction of the repulsive region as a grows, leading to larger integrated infall times. Conversely, counter-rotating families ($\lambda < 0$) can intersect attractive domains even for relatively large $|a|$, yielding shorter infall times. As the energy increases, the attractive region expands and dominates a larger fraction of parameter space, explaining why the infall times become less sensitive to a and saturate at low values. Moreover, for corotating configurations with larger angular momentum (e.g. $L = 1$), increasing a can drive the trajectory through strongly repulsive sectors, and the proper-time integral may cease to converge for some parameter choices, producing the divergent behavior seen in the numerical curves.

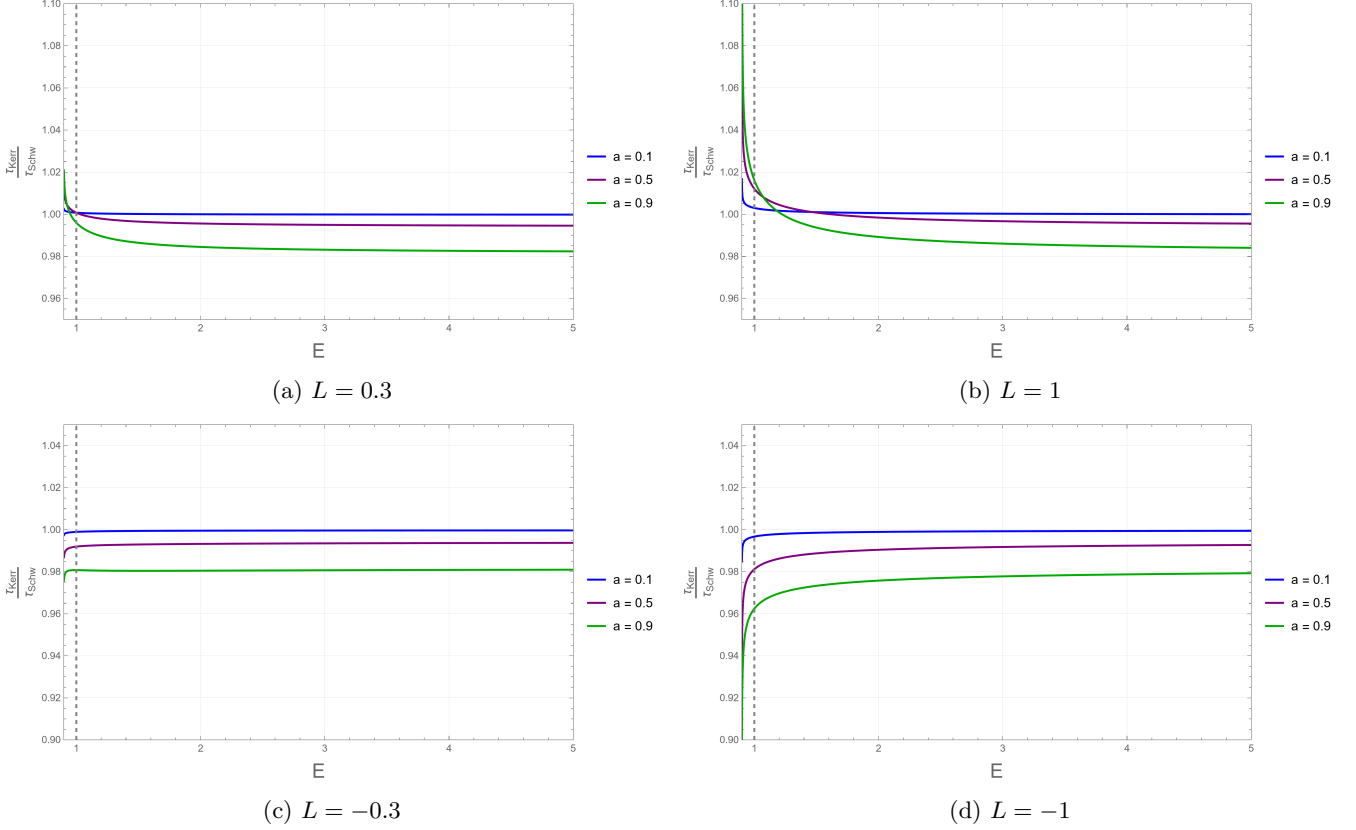


Figure 4: Ratio between Kerr and Schwarzschild values of τ for particles falling from $r_0 = 10M$ to $r_f = 3M$ in prograde (UP) and retrograde families (DOWN).

V. COVARIANT 1+3 ANALYSIS

A fully relativistic understanding of infall times requires going beyond coordinate velocities and effective potentials, and focusing instead on the covariant kinematics of geodesic congruences [3, 17, 18]. In General Relativity, the convergence or divergence of freely falling worldlines is encoded in the expansion scalar Θ , whose evolution is governed by the Raychaudhuri equation [19]. This provides a direct link between spacetime geometry and characteristic collapse times.

For a timelike geodesic congruence with four-velocity u^a , vanishing four-acceleration and zero vorticity, the Raychaudhuri equation in vacuum spacetimes ($R_{ab} = 0$) reduces to

$$\dot{\Theta} = -\frac{1}{3}\Theta^2 - \sigma_{ab}\sigma^{ab}, \quad (38)$$

where σ_{ab} is the shear tensor and the overdot denotes differentiation with respect to the proper time along the congruence. We adopt the shear scalar expressed as:

$$\sigma^2 = \sigma^{ab}\sigma_{ab} \quad (39)$$

In vacuum spacetimes, Eq. (38) shows that the local rate of focusing is controlled entirely by the expansion and the shear. More precisely, the integration of the Raychaudhuri equation along a geodesic (see e.g [3, 18]) gives the schematic relation:

$$\tau \propto \int \frac{d\Theta}{\Theta^2 + 3\sigma^2} \quad (40)$$

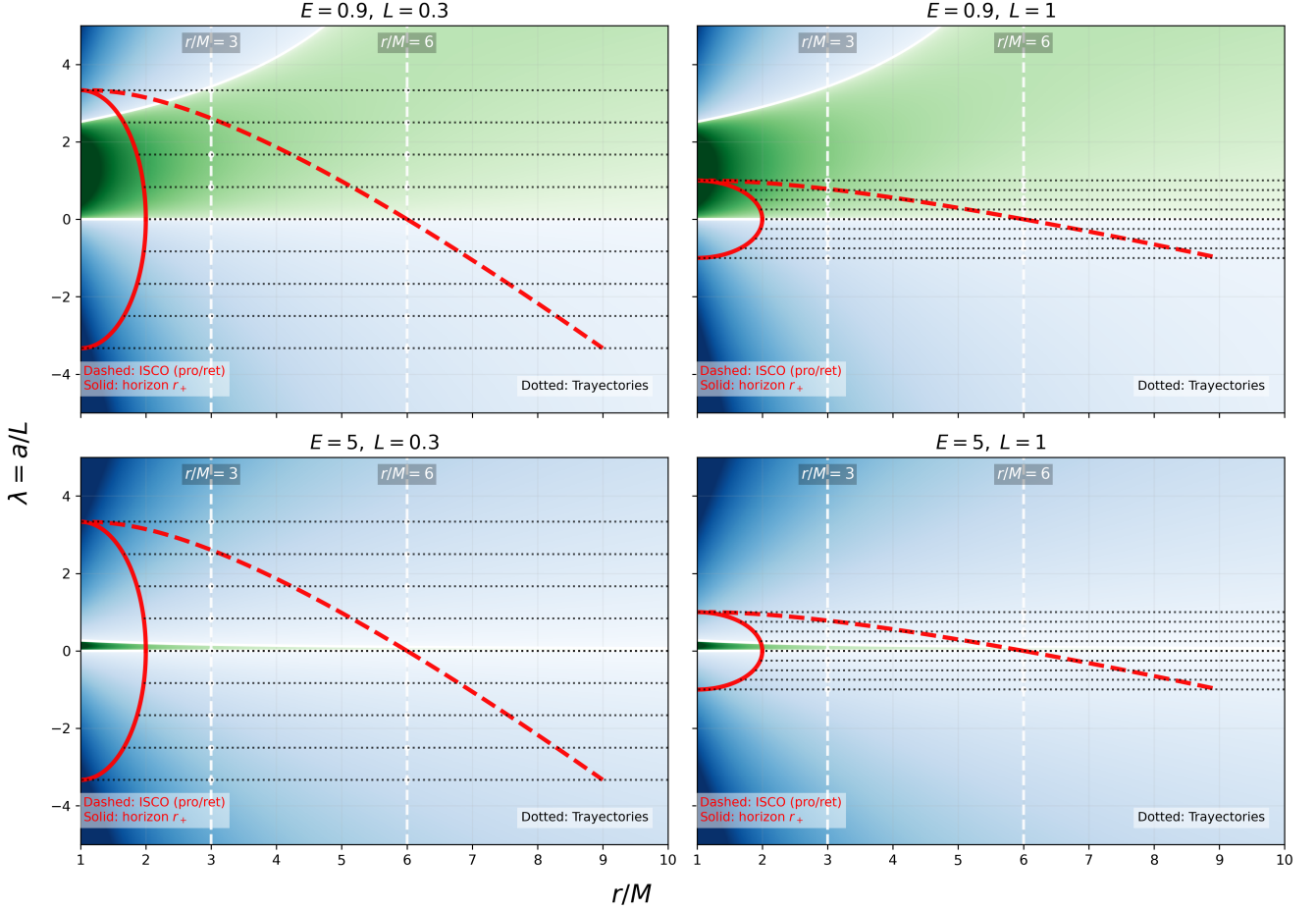


Figure 5: Parametric maps of Kerr–minus–Schwarzschild variation of the effective potential in the $(r/M, \lambda = a/L)$ plane for four representative combinations of energy E and angular momentum L . Green (blue) regions correspond to locally repulsive (attractive) contributions of the barrier sector to the radial effective potential. Dotted black curves indicate representative infall tracks from $r_0 = 10M$ toward smaller radii. The event horizon r_+ is shown as a solid red curve, while the co-rotating and counter-rotating ISCOs are shown as dashed red curves. Reference fixed radii are marked by vertical dashed white lines. The figure highlights that retrograde orbits can, at low energies, cross attractive regimes not present in the prograde case. However, the attractive regime dominates strongly the parameter space at high energies.

highlighting that proper infall times are determined by the combined effect of isotropic contraction and anisotropic distortion. In the following, we select test geodesic congruences to study the effects of the black–hole rotation in terms of covariant kinematical quantities.

A. Congruence selection

In the $1 + 3$ covariant formalism, a timelike congruence with four–velocity u^a admits a family of spacelike hypersurfaces orthogonal to its worldlines if and only if it satisfies the Frobenius integrability condition (see e.g. [3, 20])

$$u_{[a} \nabla_b u_{c]} = 0, \quad \iff \quad \omega_{ab} = 0, \quad (41)$$

where the vorticity tensor is defined by

$$\omega_{ab} \equiv h_a^c h_b^d \nabla_{[d} u_{c]}, \quad h_{ab} \equiv g_{ab} + u_a u_b \quad (42)$$

and projects orthogonally to u^a .

In stationary and axisymmetric spacetimes such as Schwarzschild and Kerr, the Killing vectors ∂_t and ∂_ϕ imply two constants of motion along geodesics, the specific energy $E \equiv -p_t$ and the specific angular momentum $L \equiv p_\phi$. It is therefore natural to consider congruences of freely falling test particles characterized by fixed values of E and L . For such congruences, the Frobenius condition (41) ensures that fixing L does not, by itself, introduce vorticity: a congruence with uniform specific angular momentum can be irrotational, even though individual worldlines carry angular motion with respect to asymptotic observers. As a result, any rotational effects in the Raychaudhuri dynamics arise from anisotropic tidal distortions (shear) rather than from intrinsic vorticity. This property has a transparent Newtonian analogue that helps build intuition. Consider an axisymmetric velocity field in classical mechanics with purely azimuthal motion and constant specific angular momentum with respect to the symmetry axis, $v_\phi = L/\rho$, where ρ is the cylindrical radius. The Newtonian vorticity is then

$$(\nabla \times \mathbf{v})_z = \frac{1}{\rho} \frac{\partial}{\partial \rho} (\rho v_\phi) = \frac{1}{\rho} \frac{\partial}{\partial \rho} \left(\rho \frac{L}{\rho} \right) = 0, \quad (\rho \neq 0), \quad (43)$$

showing that the flow is locally irrotational (except at the axis, where a topological singularity may appear). In this sense, a flow with constant specific angular momentum does not generate Coriolis-like effects associated with vorticity; such effects arise only when the angular velocity itself varies across neighboring streamlines. The relativistic condition $\omega_{ab} = 0$ plays the direct analogue of this statement: for congruences with fixed E and L , the absence of vorticity implies that frame-dragging and rotation influence the dynamics through shear and expansion, rather than through local rotational twisting of the congruence.

B. Illustrative case with $L = 0$

As an illustrative example, in the Schwarzschild spacetime, a congruence characterized by a fixed specific energy E and vanishing angular momentum $L = 0$ has a radial component of the four-velocity

$$\dot{r} = -\sqrt{E^2 - 1 + \frac{2M}{r}}, \quad (44)$$

A direct covariant calculation yields the expansion scalar

$$\Theta_{\text{Schw}}(r) = -\frac{2}{r} \sqrt{E^2 - 1 + \frac{2M}{r}} + \frac{M}{r^2 \sqrt{E^2 - 1 + \frac{2M}{r}}}, \quad (45)$$

which is negative everywhere along the infall, reflecting the convergence of neighboring worldlines. Note that an increase in Θ corresponds to a reduction in the magnitude of the contraction rate, since Θ is negative for infalling congruences.

Since the congruence is geodesic and irrotational, the shear magnitude follows directly from the Raychaudhuri equation,

$$\sigma_{\text{Schw}}^2(r) = -\dot{\Theta}_{\text{Schw}} - \frac{1}{3} \Theta_{\text{Schw}}^2, \quad (46)$$

yielding an explicit expression that depends only on r , M and E . In Schwarzschild, this shear has a purely tidal origin and reflects the familiar radial stretching and angular squeezing of infalling geodesics. In contrast, for equatorial geodesics in the Kerr spacetime the expansion scalar of the congruence is

$$\Theta_{\text{Kerr}}(r) = -\frac{2}{r} \sqrt{F_{\text{Kerr}}(r)} + \frac{1}{\sqrt{F_{\text{Kerr}}(r)}} \left(\frac{M}{r^2} + \frac{a^2(E^2 - 1)}{r^3} + \frac{3Ma^2E^2}{r^4} \right), \quad (47)$$

Where:

$$F_{\text{Kerr}}(r) = E^2 - 1 + \frac{2M}{r} + \frac{a^2(E^2 - 1)}{r^2} + \frac{2Ma^2E^2}{r^3}. \quad (48)$$

Comparing Eqs. (45) and (47), one sees that rotation reduces or increases the magnitude of the expansion at fixed radius, depending on the energy. In particular, for large energies (which correspond to a reduction in proper infalling times), $F_{\text{Kerr}} \sim E^2$ and the magnitude of Θ can be approximated by:

$$\Theta_{\text{Kerr}} \sim E \left[-\frac{2}{r} + a^2 \left(\frac{1}{r^3} + \frac{3M}{r^4} \right) \right], \quad (E \gg 1). \quad (49)$$

naively, as a grows, Θ is systematically reduced in magnitude (more positive). If one were to assess the infall dynamics based on the expansion alone, this behaviour would suggest a slower local convergence of the congruence and, consequently, a tendency toward larger proper infall times.

The last statement seems to be in tension with the heuristic analysis, since we have seen that for high E , a contributes attractively to the effective potential, decreasing τ . However, the Raychaudhuri equation shows that the rate of focusing is not controlled by Θ alone, but by the combination

$$\frac{1}{3}\Theta^2 + \sigma^2. \quad (50)$$

Using Eq. (38), the shear magnitude in Kerr can again be obtained directly from $\Theta_{\text{Kerr}}(r)$,

$$\sigma_{\text{Kerr}}^2(r) = -\dot{\Theta}_{\text{Kerr}} - \frac{1}{3}\Theta_{\text{Kerr}}^2. \quad (51)$$

C. Numerical results

In Figs. 6 and 7 we illustrate how Kerr rotation modifies the geometric structure of a timelike geodesic congruence with fixed $|L| = 0.3$, for moderately relativistic ($E = 0.95$) and highly relativistic ($E = 5$) regimes, respectively. A high spin parameter $a = 0.9$ is chosen in order to enhance and clearly expose the rotational effects.

A key result is that, although Kerr rotation systematically makes the expansion scalar Θ less negative (thereby reducing the magnitude $|\Theta|$ relative to Schwarzschild), it simultaneously induces significant and energy-dependent modifications to the shear. For moderate energies ($E = 0.95$, Fig. 6), prograde congruences exhibit a reduction of the shear with respect to Schwarzschild, leading to a weaker focusing and hence to an increase of the integrated proper time τ [Eq. (40)]. In contrast, retrograde congruences display an enhanced shear, which strengthens the focusing and reduces τ .

At higher energies ($E = 5$, Fig. 7), this behaviour changes qualitatively: Kerr rotation enhances the shear for both prograde and retrograde congruences, leading in both cases to a stronger focusing and shorter infall times. These results provide a fully covariant explanation for why Kerr rotation can either lengthen or shorten proper infall times, even when the local expansion magnitude is reduced. Rather than acting as a simple centrifugal barrier or as a purely attractive correction, black-hole rotation redistributes the gravitational influence between isotropic convergence, encoded in Θ , and anisotropic tidal distortions, encoded in the shear. The competition between these two effects, as captured by the Raychaudhuri equation, ultimately controls the rate of gravitational focusing and the resulting infall times.

VI. DISCUSSION

The analysis developed in this work shows that, in General Relativity, angular momentum does not play a purely centrifugal role. Instead, through its relativistic couplings with energy and spacetime rotation, it can either weaken or enhance the effective gravitational attraction experienced by infalling matter. By combining an effective-potential decomposition with fully integrated infall times, we have identified well-defined regions of parameter space in which black-hole rotation systematically reduces the proper free-fall time relative to the Schwarzschild case. Although this effect is subdominant compared to the overall energetic dependence of the infall, it is physically transparent, and potentially relevant in specific astrophysical regimes.

From the numerical results obtained for fixed final radii, we find that the relative correction induced by rotation typically satisfies

$$\frac{\Delta\tau}{\tau_{\text{Schw}}} \equiv \frac{\tau_{\text{Kerr}} - \tau_{\text{Schw}}}{\tau_{\text{Schw}}} \sim 10^{-2} - 10^{-1}, \quad (52)$$

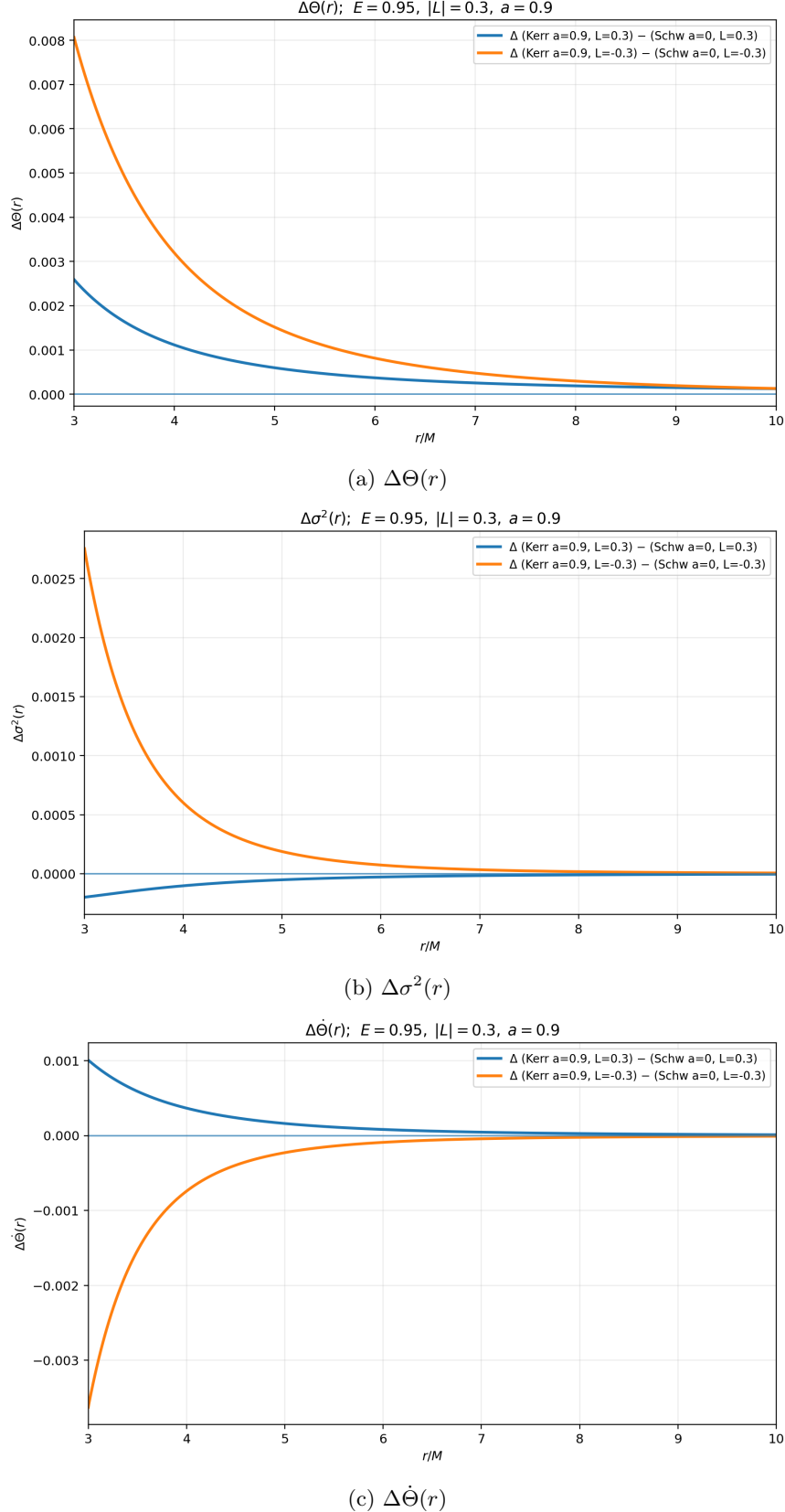


Figure 6: Differences between Kerr and Schwarzschild congruence kinematics for moderately relativistic infall with $E = 0.95$, $|L| = 0.3$ and $a = 0.9$. Each panel shows the radial dependence of $\Delta X(r) \equiv X_{\text{Kerr}}(r) - X_{\text{Schw}}(r)$, with blue curves corresponding to prograde orbits ($aL > 0$) and orange curves to retrograde orbits ($aL < 0$). Although

Kerr rotation increases the expansion magnitude ($\Delta\Theta > 0$) in both cases, it affects the shear in an opposite manner: $\Delta\sigma^2 < 0$ for prograde orbits and $\Delta\sigma^2 > 0$ for retrograde ones. This asymmetric shear modulation leads to qualitatively different focusing behaviour, as captured by $\Delta\dot{\Theta}$.

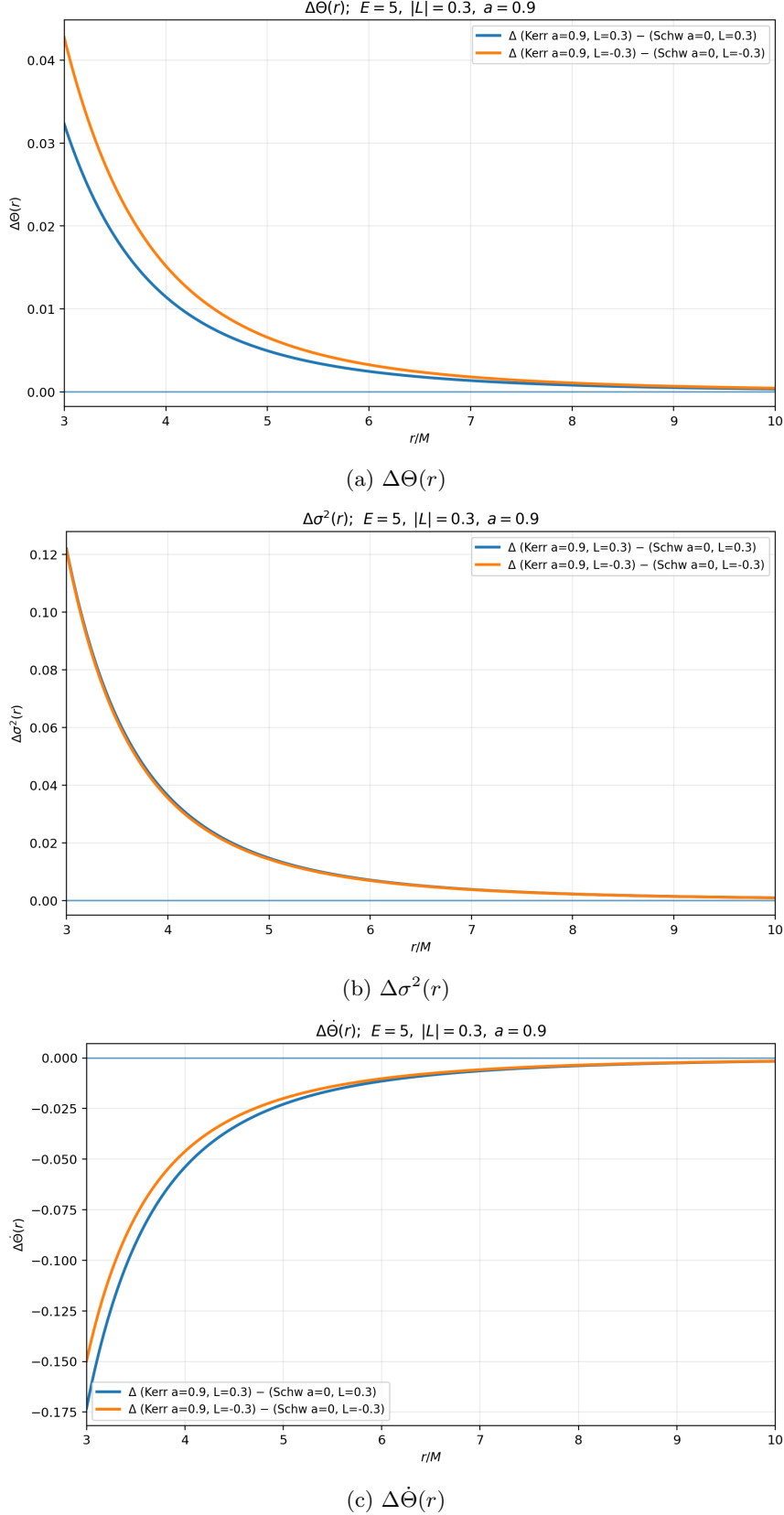


Figure 7: Same as Fig. 6, but for highly relativistic infall with $E = 5$. In this regime the shear enhancement induced by Kerr rotation becomes dominant for prograde orbits, while the corresponding focusing rate $\dot{\Theta}$ becomes more negative than in the Schwarzschild case. This inversion relative to the low-energy behaviour demonstrates that the impact of rotation on gravitational focusing is controlled primarily by the energy-dependent modulation of the shear, rather than by the expansion alone.

depending on the spin parameter a , the specific angular momentum L , and the energy regime considered. While modest in magnitude, this correction has a systematic sign and therefore may accumulate in prolonged or repeated infall processes. For a supermassive black hole of mass $M \sim 10^8 M_\odot$, the natural gravitational timescale is

$$t_M \equiv \frac{GM}{c^3} \sim 10^3 \text{ s}, \quad (53)$$

which corresponds to the light-crossing time of one gravitational radius. Proper free-fall times from tens of gravitational radii are typically of order $\mathcal{O}(10^2\text{--}10^3) t_M$, that is, of order days to weeks. A relative correction at the percent level then translates into absolute differences of hours to days in characteristic infall times. Such timescales are negligible from a cosmological standpoint, but they can be relevant for local dynamical processes. In particular, our results show that in regimes characterized by low specific angular momentum and sufficiently high energy, black-hole rotation can enhance the effective radial infall, leading to systematically shorter proper collapse times than in a non-rotating spacetime.

From a fully covariant perspective, the results presented here can be understood as a direct manifestation of Raychaudhuri dynamics for timelike geodesic congruences. In General Relativity, for zero vorticity congruences, the rate at which neighboring worldlines converge is not controlled by gravitational attraction alone, but by the interplay between the expansion scalar and the shear of the congruence. Although Kerr rotation can locally reduce the magnitude of the expansion relative to Schwarzschild, it simultaneously enhances the anisotropic tidal distortions encoded in the shear. As a result, the covariant focusing term $\frac{1}{3}\Theta^2 + \sigma^2$ may be either strengthened or weakened, depending on the energy, angular momentum and radius, leading to systematic modifications of the integrated proper infall time. In this sense, the spin-induced enhancement or suppression of infall identified in this work is not a coordinate-dependent velocity effect, but a genuinely geometric consequence of how relativistic kinematics and spacetime rotation reshape the local deformation of geodesic bundles.

This conclusion immediately clarifies where the effect is, and is not, expected to play a role. In standard thin accretion disks around stellar-mass and supermassive black holes, described by the Shakura–Sunyaev and Novikov–Thorne models [21, 22], the gas follows nearly Keplerian orbits with large angular momentum and bound energies outside the ISCO. In this regime, the dimensionless ratio $\mu = aE/L$ is typically small, the centrifugal barrier remains dominant, and the relativistic term proportional to $(L - aE)^2/r^3$ does not overcome it. Consistently with the standard picture, the influence of spin in thin disks manifests primarily through the shift of the ISCO radius and the associated change in radiative efficiency, rather than through a direct enhancement of gravitational infall.

The situation is qualitatively different in accretion flows with low angular momentum, such as quasi-spherical inflows or advection-dominated accretion flows (ADAFs) [23, 24]. In these configurations, the centrifugal barrier is weakened and the relativistic coupling between energy, angular momentum and spin can become dynamically important. In particular, the enhancement of radial velocities in low- L , high-spin configurations reported by [13] finds a natural interpretation within the effective-potential framework developed here. While realistic ADAFs are governed by hydrodynamics, viscosity and pressure support, the present analysis isolates a purely relativistic kinematical effect that operates in the same low-angular-momentum regime.

An especially interesting application arises in scenarios for the formation of massive black-hole seeds in protogalactic halos at high redshift. In direct-collapse models, fragmentation is suppressed and a significant fraction of the baryonic mass flows toward the center [25–28]. Numerical simulations and analytic arguments indicate that, during the most violent collapse phases, portions of the gas may follow non-Keplerian, nearly radial trajectories with relatively low specific angular momentum. From the perspective of the Kerr effective potential, such configurations are precisely those in which the relativistic spin-dependent terms can compete effectively with the centrifugal barrier. For sufficiently large values of $\mu = aE/L$, and for energies exceeding the critical thresholds identified in this work, black-hole rotation acts to increase the effective attraction and shorten infall times compared to the non-rotating case. Unlike thin disks, where spin mainly shifts the ISCO, here the rotation can directly enhance the accretion dynamics itself. While modest in magnitude, such relativistic effects may become relevant during repeated infall episodes or sustained low-angular-momentum phases.

By contrast, systems such as extreme mass-ratio inspirals (EMRIs) [29, 30] remain firmly in the high-angular-momentum regime throughout their evolution. In these cases, the centrifugal barrier always dominates the radial dynamics, even near the ISCO, and the infall never becomes quasi-radial. Accordingly, EMRIs do not probe the enhanced gravitational regime identified here.

Beyond specific astrophysical systems, our results connect naturally with a broader relativistic principle: in General Relativity, motion itself gravitates. At the microscopic level, this is explicit in kinetic theory, where pressure arises from momentum transport [31]. At the macroscopic level, pressure, energy fluxes, and stresses all enter the energy-momentum tensor and contribute to the gravitational field. In cosmology, this idea is well known

through the appearance of $\rho + 3p$ in the Friedmann equations and through the Tolman–Oppenheimer–Volkoff balance in compact stars [2, 3].

More recently, Tsagas and collaborators have shown within the covariant $1 + 3$ formalism that large-scale peculiar velocities and the associated energy flux q_a act as additional gravitational sources, modifying the growth of inhomogeneities relative to Newtonian expectations [6, 7, 32]. The spin–induced enhancement of infall identified in Kerr represents another manifestation of this same principle. Here, it is the orbital motion and frame dragging associated with spacetime rotation that contribute to the effective gravitational pull. Although the local Kerr dynamics studied in this work and the cosmological tilted–observer effects operate on very different scales, both illustrate how relativistic kinematics can modify collapse and growth times relative to the Newtonian picture. In environments relevant for early structure formation, one may speculate that the combined action of local spin–induced dynamics around compact objects and large-scale relativistic energy fluxes could further amplify effective collapse rates. A unified treatment incorporating both effects lies beyond the scope of the present work, but represents a natural and intriguing direction for future research.

Overall, our results emphasize that even in the test–particle limit, General Relativity admits regimes in which angular momentum and motion strengthen rather than oppose gravitational collapse. While the magnitude of the effect is modest, its systematic nature and clear physical origin make it a useful benchmark for assessing relativistic corrections to infall, accretion, and growth timescales in more complex astrophysical and cosmological settings.

VII. CONCLUSIONS

In this work we have explored how General Relativity modifies gravitational infall relative to the Newtonian picture, using the Schwarzschild and Kerr spacetimes as controlled theoretical laboratories. Our focus has been on free–fall timescales and on the role played by particle energy, orbital angular momentum, and black–hole spin in shaping the efficiency of collapse. Rather than aiming at detailed astrophysical modelling, our goal has been to identify and interpret regimes in which genuinely relativistic effects arise and to clarify their dynamical and geometric origin.

By analysing the radial effective potential, we have shown that relativistic infall cannot be understood as a simple competition between Newtonian attraction and a classical centrifugal barrier. Even in the non–rotating Schwarzschild spacetime, angular momentum does not act as a purely repulsive agent: the relativistic correction proportional to $-ML^2/r^3$ systematically weakens the centrifugal barrier. As a result, trajectories with non–zero angular momentum experience shorter proper fall times than predicted by Newtonian dynamics, highlighting that relativistic kinematics already alters collapse timescales even in the absence of rotation.

The Kerr spacetime introduces a qualitatively richer structure. The appearance of the combination $(L - aE)$ in the effective potential leads to a direct coupling between orbital angular momentum, particle energy, and black–hole spin. This spin–orbit–energy coupling fundamentally modifies the classical role of angular momentum. Depending on the sign and magnitude of L relative to a , and on the energetic regime of the trajectory, the angular–momentum contribution can become effectively attractive rather than repulsive. In particular, for sufficiently high energies and low orbital angular momentum, black–hole rotation opens access to more attractive regions of the potential, thereby favouring radial infall and reducing collapse times relative to the Schwarzschild case.

Our numerical integrations of the proper infall time toward fixed final radii confirm that these modifications of the effective potential have tangible dynamical consequences once complete trajectories are considered. For corotating and counter–rotating configurations, the total proper fall time can be either shortened or lengthened relative to Schwarzschild, depending on the interplay between energy, angular momentum and spin. These trends are in full agreement with the local attractive and repulsive regimes identified in the effective–potential analysis, and demonstrate that black–hole rotation introduces a genuinely relativistic correction to infall dynamics beyond purely energetic considerations.

From a covariant standpoint, these results admit a natural interpretation in terms of the Raychaudhuri dynamics of timelike geodesic congruences. In General Relativity, the rate at which neighboring worldlines focus is governed not only by the local expansion of the congruence, but by the combined action of expansion and shear. While Kerr rotation can locally reduce the magnitude of the expansion relative to Schwarzschild, it simultaneously enhances the anisotropic tidal distortions encoded in the shear. As a result, the focusing term $\frac{1}{2}\Theta^2 + \sigma^2$ may be either strengthened or weakened, depending on energy, angular momentum and radius. This covariant balance provides a unified explanation for why black–hole rotation can lead to either shorter or longer proper infall times, despite a reduced local expansion.

From a broader conceptual perspective, our results reinforce a central lesson of General Relativity: motion itself

gravitates. The spin–orbit coupling identified in Kerr represents a concrete manifestation of this principle, closely related to the gravitational role played by pressure in compact objects or by energy fluxes in relativistic cosmology. In all these cases, not only rest–mass energy but also kinetic energy, angular momentum and associated energy flows contribute to the effective gravitational field and can modify characteristic collapse and growth timescales.

While the present analysis does not aim to explain complex astrophysical phenomena such as the early formation of galaxies or supermassive black holes, it identifies well–defined regimes in which purely relativistic effects associated with rotation can systematically shorten or lengthen collapse times relative to Newtonian or quasi–Newtonian expectations. In idealised scenarios characterised by low centrifugal support and quasi–radial flows, such effects may act as a complementary mechanism that favours rapid infall and early growth.

Finally, this work should be regarded as a first exploratory step. The analysis has been restricted to test–particle dynamics and neglects hydrodynamics, viscosity, radiation and feedback. Natural extensions include the study of generic non–equatorial trajectories, the explicit computation of shear and expansion for more general congruences, and the exploration of the combined impact of local spin–induced effects and large–scale relativistic flows in cosmological environments. In this sense, revisiting gravitational infall timescales within full General Relativity provides a clean and conceptually transparent framework for isolating kinematical relativistic mechanisms that may contribute to structure formation and to the interpretation of massive compact objects in the early Universe.

ACKNOWLEDGEMENTS

The author thanks Christos G. Tsagas for insightful discussions and valuable comments that helped clarify the covariant interpretation of the results presented in this work.

[1] P. J. E. Peebles, *The large-scale structure of the universe* (1980).

[2] C. W. Misner, K. S. Thorne, and J. A. Wheeler, *Gravitation* (W. H. Freeman, 1973).

[3] R. M. Wald, *General Relativity* (University of Chicago Press, 1984).

[4] S. M. Carroll, *Spacetime and Geometry: An Introduction to General Relativity* (Cambridge University Press, 2019).

[5] J. B. Hartle, *Gravity : an introduction to Einstein's general relativity* (2003).

[6] K. Filippou and C. G. Tsagas, *Astrophysics and Space Science* **366**, 10.1007/s10509-020-03912-4 (2021).

[7] E. Tsaprazi and C. G. Tsagas, *The European Physical Journal C* **80**, 10.1140/epjc/s10052-020-8312-0 (2020).

[8] K. Schwarzschild, *Sitzungsberichte der Königlich Preussischen Akademie der Wissenschaften* , 189 (1916).

[9] R. P. Kerr, *Phys. Rev. Lett.* **11**, 237 (1963).

[10] R. H. Boyer and R. W. Lindquist, *Journal of Mathematical Physics* **8**, 265 (1967).

[11] B. Carter, *Physical Review* **174**, 1559 (1968).

[12] S. Chandrasekhar, *The Mathematical Theory of Black Holes* (Oxford University Press, 1983).

[13] S. Das and S. K. Chakrabarti, *Monthly Notices of the Royal Astronomical Society* **389**, 371 (2008), <https://academic.oup.com/mnras/article-pdf/389/1/371/18429946/mnras0389-0371.pdf>.

[14] M. Boylan-Kolchin, *Nature Astronomy* **7**, 731 (2023), arXiv:2208.01611.

[15] C. A. Mason, M. Trenti, and T. Treu, *Monthly Notices of the Royal Astronomical Society* **521**, 497 (2023).

[16] J. M. Bardeen, W. H. Press, and S. A. Teukolsky, *The Astrophysical Journal* **178**, 347 (1972).

[17] C. TSAGAS, A. CHALLINOR, and R. MAARTENS, *Physics Reports* **465**, 61–147 (2008).

[18] E. Poisson, *A Relativist's Toolkit: The Mathematics of Black-Hole Mechanics* (Cambridge University Press, 2009).

[19] A. K. Raychaudhuri, *Phys. Rev.* **98**, 1123 (1955).

[20] G. F. R. Ellis, R. Maartens, and M. A. H. MacCallum, *Relativistic Cosmology* (Cambridge University Press, 2012).

[21] N. I. Shakura and R. A. Sunyaev, *Astronomy and Astrophysics* **24**, 337 (1973).

[22] I. D. Novikov and K. S. Thorne, in *Black Holes (Les Astres Occlus)*, edited by C. DeWitt and B. S. DeWitt (Gordon and Breach, 1973) pp. 343–450.

[23] R. Narayan and I. Yi, *The Astrophysical Journal Letters* **428**, L13 (1994).

[24] M. A. Abramowicz, X.-M. Chen, M. Granath, and J.-P. Lasota, *The Astrophysical Journal* **471**, 762 (1996).

[25] M. C. Begelman, M. Volonteri, and M. J. Rees, *Monthly Notices of the Royal Astronomical Society* **370**, 289 (2006).

[26] V. Bromm and A. Loeb, *The Astrophysical Journal* **596**, 34 (2003).

[27] M. A. Latif and A. Ferrara, *Publications of the Astronomical Society of Australia* **33**, e051 (2016).

[28] M. Volonteri, *Astronomy and Astrophysics Review* **18**, 279 (2010).

[29] L. Barack and C. Cutler, *Physical Review D* **69**, 082005 (2004).

[30] P. Amaro-Seoane, J. R. Gair, M. Freitag, and et al., *Classical and Quantum Gravity* **24**, R113 (2007).

- [31] S. Weinberg, *Gravitation and Cosmology: Principles and Applications of the General Theory of Relativity* (Wiley, 1972).
- [32] C. G. Tsagas, Physical Review D **84**, [10.1103/physrevd.84.063503](https://doi.org/10.1103/physrevd.84.063503) (2011).